AIAA JOURNAL
Vol. 39, No. 7, July 2001

Study of Interlaminar Stresses in Composite Laminates Subjected to Torsional Loading

John A. Mitchell* and J. N. Reddy†
Texas A&M University, College Station, Texas 77843-3123

A computational procedure for accurate determination of interlaminar stresses in thick and thin composite laminates subjected to torsional loading is presented. A multilevel, recursively defined preconditioner in conjunction with the preconditioned conjugate gradient (PCG) algorithm is constructed from a sequence of hierarchical vector spaces arising from the *p*-version of the finite element method. The computational procedure is used to model stress fields in thick and thin laminates in torsion using three-dimensional and quasi-three-dimensional models. Results indicate that the preconditioner developed here can be used to produce an efficient iterative solver for the determination of two- and three-dimensional stress fields in composite structures.

I. Introduction

A. Background

FIBER-REINFORCED composite laminates often have low transverse shear stiffness and thus exhibit significant transverse shear deformation. They also exhibit transverse stress concentrations near material and geometric discontinuities (the so-called free-edge effect) that can lead to damage in the form of matrix cracking and delamination. Finite element analyses of thin plates are plagued by overstiffening of the equations, termed *locking*, and can be improved by using refined meshes or rational modifications of the computational model. In applications where a high degree of accuracy from finite element approximations is required, discretization is increased to ever smaller scales, and the polynomial order of interpolation on elements may also be increased. This level of discretization produces extreme memory demands on traditional direct solution methods that require assembly of the global stiffness matrix, thus inhibiting the solution of such problems. However, the preconditioned conjugate gradient (PCG) algorithm is an iterative method for solving systems of algebraic equations. Its ease of implementation, low storage requirements, and rate of convergence make the PCG method an attractive approach to the solution of these very large-sized problems. However, the rate of convergence of the algorithm is directly related to the quality of the preconditioner. In the absence of a good preconditioner, the rate of convergence may deteriorate to a point at which the algorithm is not competitive with other solution methodologies.

The present study deals with the development of an efficient preconditioner for the PCG method and its application to the stress analysis of laminates subjected to torsion. Three-dimensional elasticity and quasi-three-dimensional models of the problem are used in conjunction with the finite element method and PCG algorithm to study the interlaminar stress fields in thin and thick laminates. The following brief review of literature on preconditioners and the torsion problem provides the background for the present study.

B. Literature Review

A preconditioner is an approximation to the inverse of the matrix problem being solved. To be of practical use, it should be inexpensive to compute and have few memory requirements. In practice, some tradeoffs between memory requirements and the quality of the resulting preconditioner must be considered. Most preconditioners have a substantial content of direct solution procedures embedded within them.

There are many published works on iterative solvers for elliptic problems, and it is not possible to completely cover the vast amount of literature on the subject. Most rely on the PCG algorithm and focus on construction of useful preconditioners. There are many types of preconditioners, most of which fall into one of the following categories: domain decomposition,[1,2] multigrid,[3–6] hierarchical basis,[7–11] and incomplete factorization preconditioners.[12,13] In addition to these broad classifications, there are hybrid preconditioners that mix and match features from each of the categories. Although the preconditioners can be classified into groups, there is a certain amount of commonality in that they contain some amount of direct solution procedures.

Stress analysis of laminates is difficult primarily because of the level of mesh refinement that is required to achieve a high degree of accuracy. This is especially true for torsion of laminated bars with rectangular cross sections, which is the subject of the present study. To keep element span ratios within reason, it is necessary to have a large number of elements along the length of the bar because the length dimension is much larger than the cross-sectional dimensions. For this reason, quasi-three-dimensional models have been developed to reduce the computational cost of a three-dimensional analysis.[14] Pipes and Pagano[15] first used the model for analyzing laminates under uniaxial extension and discovered the so-called free-edge effect, which causes delaminations. Later, Chan and Ochoa[16] and Leger and Chan[17] used the model to study laminates under more general loading conditions, including torsion. Chan and Ochoa used the model to study energy release rates in laminates with delaminations. They also studied stacking sequences in symmetric laminates and their effect on interlaminar stress distributions under bending and torsion loads. Leger and Chan studied both symmetric and unsymmetric laminates under uniaxial extension, bending, torsion, and out-of-plane bending loads. Following this work, Liao and Sun[18] used the Chan and Ochoa model to study thick laminates with a large number of plies by replacing the large number of individual laminae with effective moduli so that the computational cost could be reduced.

There is a slight difference between the models used by Chan and Ochoa and later by Leger and Chan. The Leger and Chan model uses a displacement field that has the same form as that obtained by integrating the equilibrium equations. Chan and Ochoa used the same displacement field, except that they ignored one term in the displacement component u along the x direction. This difference between the two models affects the interlaminar shear strain ϵ_{xz}. The twisting curvature contribution to ϵ_{xz} in the Leger and Chan model is twice that of the Chan and Ochoa model.

In addition to the above numerical studies, experiments on laminates subjected to torsional loads have been conducted.[19,20] These studies indicate that interlaminar shear stresses, σ_{xz} and σ_{yz}, are critical to the onset of shear stress failures for laminates in torsion.

Received 28 February 1998; revision received 10 May 2000; accepted for publication 20 August 2000.

*Graduate Research Assistant; currently Senior Member Technical Staff, Sandia National Laboratory, P.O. Box 5800, MS 0443, Albuquerque, NM 87185-0443.

†Distinguished Professor and Holder of the Oscar S. Wyatt Endowed Chair, Department of Mechanical Engineering. Associate Fellow AIAA.

The accuracy of the analytical prediction of such failures depends on the accuracy of the interlaminar stress field. In the present study, attention is focused on this aspect.

II. Multilevel, Hierarchical-Basis Preconditioner

A. Exact and Finite Element Models

Consider the variational problem of finding the displacement vector $\boldsymbol{u} \in H$ such that

$$a(\boldsymbol{u}, \boldsymbol{v}) = F(\boldsymbol{v}) \qquad \text{for all} \qquad \boldsymbol{v} \in \boldsymbol{H} \tag{1}$$

$$\boldsymbol{H} = \left\{ \boldsymbol{u} = (u_1, u_2, u_3) \in H^1(\Omega) \times H^1(\Omega) \times H^1(\Omega) : \boldsymbol{u} = 0 \text{ on } \Gamma_1 \right\} \tag{2}$$

where $\Omega \subset \Re^3$ denotes the domain with the boundary Γ, and Γ_1 is the portion of Γ on which the displacement vector $\boldsymbol{u}$ is specified. Here $a(\cdot, \cdot)$ denotes a bilinear form and $F(\cdot)$ denotes the linear functional associated with the boundary-value problem at hand, H^m denotes the Sobolev space of order m (see Refs. 21 and 22).

In the finite element method,[22–25] we seek an approximation of $\boldsymbol{u}$ in a finite-dimensional subspace $\boldsymbol{W}_J$ of $\boldsymbol{H}$ (or $W_J \subset H$): find $\boldsymbol{u}_J \in \boldsymbol{W}_J$ such that

$$a(\boldsymbol{u}_J, \boldsymbol{v}) = F(\boldsymbol{v}) \quad \text{for all} \quad \boldsymbol{v} \in \boldsymbol{W}_J \tag{3}$$

Let $\{\phi_i\}$ $(i = 1, 2, \ldots, n_J)$ denote a basis for $W_J \subset H^1(\Omega)$. The algebraic problem arising from Eq. (3) can be written as

$$\boldsymbol{A}_J \boldsymbol{u}^J = \boldsymbol{b} \tag{4}$$

where components of the matrix $\boldsymbol{A}_J$ and vector $\boldsymbol{b}$ are given by

$$A_J^{ij} = a(\phi_i, \phi_j), \qquad b_i = F(\phi_i), \qquad \phi_i, \phi_j \in W_J \tag{5}$$

and where components of $\boldsymbol{u}^J$ are denoted by u_j^J.

B. Conjugate Gradient Algorithm

The conjugate gradient (CG) algorithm is an iterative technique for solving the algebraic Eq. (4) when the matrix $\boldsymbol{A}$ is symmetric and positive-definite. The algorithm, its derivation, and analysis can be found in several books.[3,12] In theory, the algorithm can provide an exact solution to the problem in n steps, provided there is no round-off error. However, the algorithm is viewed here as an iterative procedure, with which a sufficiently accurate solution can be obtained in m steps, where m is much smaller than n. This acceleration of the method is achieved by using a preconditioner in the algorithm. The preconditioner is an inexpensive approximation to the inverse of $\boldsymbol{A}$, and it can significantly speed up the rate of convergence of the method. The enhanced method is the PCG algorithm. Provided that a good preconditioner can be found, the PCG algorithm is a very practical method for solving algebraic equations arising from the finite element discretization, since it can provide significant savings in both computer memory and cpu time. The CG algorithm is particularly well suited for finite element applications because of the sparseness of the stiffness matrix $\boldsymbol{A}$. The algorithm requires only computation of the action of $\boldsymbol{A}$ on the vector $\boldsymbol{u}$, and therefore matrix-vector multiplications may be computed using nonzero components of $\boldsymbol{A}$ only. Efficient implementation may be performed at the element level so that the fully assembled matrix $\boldsymbol{A}$ need not be stored.

One of the important features of the algorithm is the error estimate, which provides the rate of convergence in terms of the condition number for the problem being solved. The preconditioned version of the algorithm seeks to solve

$$\boldsymbol{NAu} = \boldsymbol{Nb} \tag{6}$$

where $\boldsymbol{N}$ denotes the preconditioner. From the analysis of the algorithm,[3,12] it is known that in s steps, the algorithm produces an approximation $\boldsymbol{u}_s$ to the exact solution $\boldsymbol{u}$ that satisfies the inequality

$$\langle \boldsymbol{e}_s, \boldsymbol{Ae}_s \rangle^{\frac{1}{2}} \leq 2 \left[\frac{\sqrt{K(\boldsymbol{NA})} - 1}{\sqrt{K(\boldsymbol{NA})} + 1} \right]^s \langle \boldsymbol{e}_0, \boldsymbol{Ae}_0 \rangle^{\frac{1}{2}} \tag{7}$$

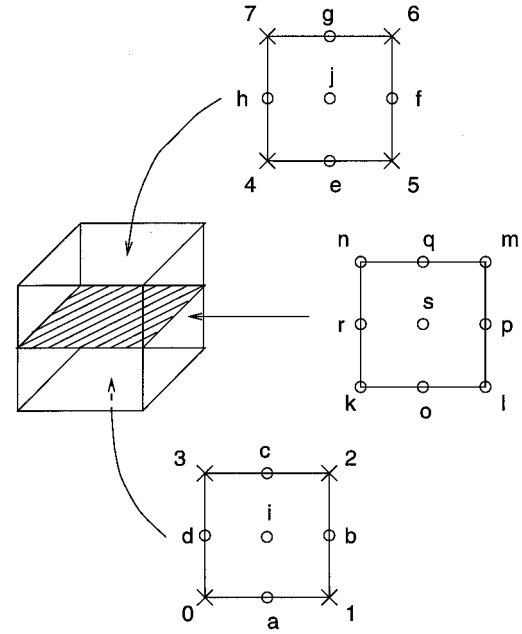

Fig. 1 Master brick element.

where $\langle \cdot, \cdot \rangle$ denotes the Euclidean inner product, $\boldsymbol{e}_s = \boldsymbol{u}_s - \boldsymbol{u}$, and $K(\boldsymbol{NA})$ represents the condition number of $\boldsymbol{NA}$. The condition number of a matrix $\boldsymbol{B}$ is defined as the ratio of the largest eigenvalue to the smallest eigenvalue of $\boldsymbol{B}$, so that $K(\boldsymbol{B}) = \lambda_{\max}/\lambda_{\min}$. Assuming that $\boldsymbol{N} = \boldsymbol{A}^{-1}$, then $K(\boldsymbol{NA}) = 1$, and the PCG algorithm converges in one step. Therefore, we are looking for a preconditioner $\boldsymbol{N}$ that is a good approximation to $\boldsymbol{A}^{-1}$. If this is the case, then $K(\boldsymbol{NA}) \approx 1$, and the algorithm will converge very quickly.

C. Elemental Basis Functions

The variational problem in Eq. (3) requires that the finite element approximation be C^0 continuous in order to ensure finite strain energy. Over each element, polynomials are used to approximate the solution, and the global finite element solution is produced by element assembly, which enforces solution continuity across interelement boundaries and thus produces a global finite element approximation that has C^0 continuity. In this section, the basis functions for a brick element used to approximate solutions in three dimensions are described.

The master brick element shown in Fig. 1 has 27 nodes for polynomial orders of quadratic and higher. It is convenient to distinguish shape functions according to the type of node they are associated with. The 27 nodes break down into the following node types: 8 vertex, 12 edge, 6 face, and 1 volume. Degrees of freedom at the nodes depend on the node type. For example, vertex nodes have degrees of freedom equal to function values at the element vertices, whereas an edge node has tangential derivatives up to pth order associated with the midpoint of the edge. Face nodes have degrees of freedom equal to mixed-order derivatives up to the $(p+q)$th order associated with the face node, and, analogously, volume nodes have degrees of freedom equal to mixed-order derivatives up to the $(p+q+r)$th order associated with the volume node. The approximation may be refined by increasing the order of the polynomials on the element while not introducing new nodes.

In this study, a preconditioner is constructed from a sequence of hierarchical vector spaces.[26] The sequence of hierarchical vector spaces is created by enriching elements of order p to order $(p+1)$. The incremental enrichment V_k and the original vector space W_{k-1} will be combined by direct sum to create a larger space $W_k = W_{k-1} \oplus V_k$. It is possible to create this sequence by simply using p refinement.

D. Hierarchical Vector Spaces

Here we discuss some specific sequences of vector spaces that are suitable for constructing hierarchical-basis preconditioners. First, we discuss a sequence of spaces particularly suited to thin solids.

Next we present a more general sequence for problems in which there is not one direction in the domain that is particularly thin as compared to the remaining two (e.g., three-dimensional). Last we describe a sequence of vector spaces that can be used for problems in two dimensions.

The transverse dimension of plates, beams, and shells is particularly small as compared with the other dimensions of the structure, and this leads naturally to a sequence of meaningful approximations that provide increasing accuracy by increasing the order of approximation in the transverse direction of the structure.[26] These various levels of approximation are categorized by node type and are called *node levels.* Node levels are further subdivided into hierarchical levels according to the order of interpolation at the particular node. In the case of thin solids, there are six node levels: vertex, in-plane edge, in-plane face, transverse edge, transverse face, and interior for specific node level definitions. A cutout of an example mesh shows the node levels' decomposition for a plate-type structure (Figs. 2a–2e).

The term *hierarchical level* refers to a vector space of functions defined according to the procedures discussed earlier. Node levels are simply a means for construction and discussion of the hierarchical levels. The hierarchical levels are the fundamental issue here, and there are a given number of the same within each node level for a given mesh. The vertex node level is different from the five remaining node levels in that it has only one hierarchical level corresponding to its vertex functions. A vertex node level must always exist on an element, because the vertex functions are used to model the geometry of the element. In addition, there is only one hierarchical level associated with the vertex nodes, because the vertex functions are not enriched by increasing the order of approximation associated with them. Vertex functions on the brick element are the usual trilinear shape functions. All other node levels, may have an arbitrary number of hierarchical levels, depending on the order of interpolation at the nodes.

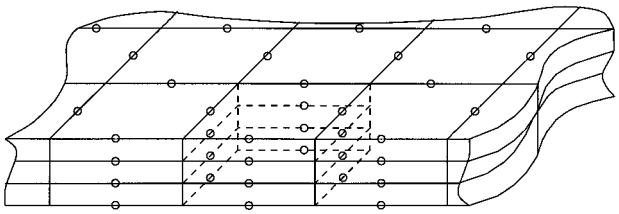

a) In-plane edges

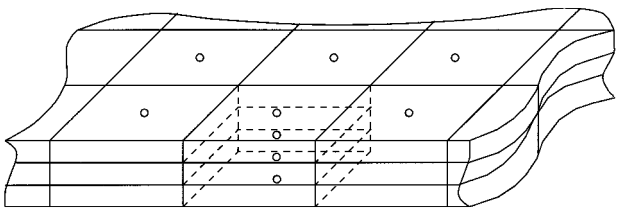

b) In-plane faces

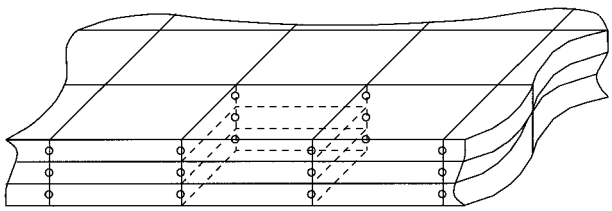

c) Transverse faces

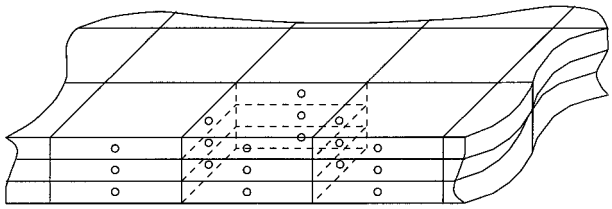

d) Transverse edges

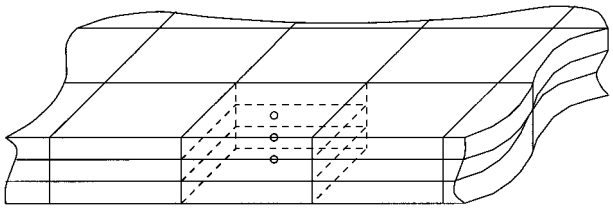

e) Volume

Fig. 2 Mesh cutout, hierarchical vector spaces, thin solids.

In the case of edges, there is one hierarchical level defined for each increment in the order of interpolation along the edge. For example, suppose that all in-plane edges have polynomial order $p = 3$. Then this node level would contribute two hierarchical levels, one for $p = 2$ and the other for $p = 3$. Transverse edges produce hierarchical levels in the same way as in-plane edges, so that in general there will be $(p - 1)$ hierarchical levels for in-plane edges and $(q - 1)$ hierarchical levels for transverse edges, assuming the transverse edges have order of interpolation q. These definitions amount to defining hierarchical levels for each type of degree of freedom because, for each increment in the order of interpolation along the edge, a new degree of freedom is introduced.

A similar procedure can be implemented for face nodes. For each new degree of freedom added at a face node through p refinement, there is a corresponding hierarchical level introduced. For instance, suppose that all in-plane face nodes have equal interpolation ($p = 3$, for example) in both local coordinate directions. Then this node has four degrees of freedom corresponding to the four different bubble functions on the face, so that in this case there would be a total of four hierarchical levels introduced, corresponding to the combinations (2, 2), (2, 3), (3, 2), and (3, 3). The treatment of in-plane face and transverse-face nodes is thereby identical.

Finally, the interior node level is treated analogously. In this case, there are many more functions involved because of the large number of degrees of freedom introduced with each incremental p refinement. As an example, suppose that an interior node has $p = 3$ in the three local coordinate directions. Then there is a total of eight hierarchical levels corresponding to the combinations (2, 2, 2), (2, 2, 3), (2, 3, 2), (2, 3, 3), (3, 2, 2), (3, 2, 3), (3, 3, 2), and (3, 3, 3).

With the hierarchical levels, defined for each node level, it is now possible to discuss the overall structure of the hierarchical levels in the context of modeling thin solids. As hierarchical levels are added to the approximation, the order of the polynomial approximation of primary variables increases. As the order of interpolation increases, it is expected that higher-frequency components are being added to the approximate solution. The order in which these refinements are made is physically meaningful.

Suppose that a beam, composed of a homogeneous material, is modeled with one element in the transverse direction and an arbitrary number of elements along the length. If the elements are taken to be linear in the thickness direction of the beam, then the finite element model closely approximates what would be captured with a finite element model of the same beam based on first-order shear deformation theory. If macroscopic response, such as transverse displacements, is of interest, this model would produce reasonably accurate results. However, if accurate stress calculations are required, some type of refinement would be necessary. In the case of the methods discussed here, the order of interpolation may be increased in the transverse direction by merely increasing the order of the polynomials associated with transverse edges to capture three-dimensional states of stress. Because of the oscillatory nature of the enhancements, an iterative solver can efficiently resolve error in the approximate solution associated with these, so that additional degrees of freedom do not dramatically increase the cost of computing the refined solution.

Next, we discuss hierarchical vector spaces for three-dimensional solids. In the preceding paragraphs, a particular sequence of subspaces that would be suitable for modeling thin solids was emphasized. The hierarchical vector spaces were constructed by

distinguishing nodes along edges and on faces in the transverse direction from nodes in the in-plane direction. However, if the problem does not have a particular direction in which the solution is expected to have a preference, then it may not be advantageous to use such a sequence of spaces. Rather, it may be better to remove this bias from the preconditioner. This is conceptually simple and amounts to treating all edges as one node level and all faces as another node level. Hierarchical levels are constructed in exactly the same manner as described in the preceding section.

Hierarchical vector spaces for two-dimensional problems can be constructed in a similar way as described for three-dimensional problems. As in the three-dimensional case, there are numerous possibilities, and much of the discussion in the preceding sections holds true for this case. For a quadrilateral element, there are only three node levels corresponding to the vertex (four), edge (four), and face (one) nodes. Again, the vertex node level must exist so that at least a linear map may be used for geometry purposes. As in the preceding cases, hierarchical levels are constructed according to the order of interpolation at the node.

E. Preconditioner

A novel preconditioner developed by Mitchell[26] is now reviewed. The preconditioner is constructed from a sequence of hierarchical vector spaces based on p refinement. In the p refinement case, the coarsest mesh level corresponds to the vector space of vertex functions. The finite element method based on p refinement seeks to obtain a good solution by fixing the mesh and increasing the polynomial order on each element. As will become clear, it is possible to obtain the increased accuracy of the p refinement procedures, but at a cost in memory corresponding to a problem in which $p = 1$.

Let W_J denote the finite-dimensional vector space corresponding to the finest level of refinement on which we seek a solution, and define the following set of subspaces W_k recursively:

$$W_1 \subset W_2 \subset W_3 \subset \cdots \subset W_J$$
$$W_k = W_{k-1} \oplus V_k \quad \text{for} \quad k = 2, 3, \ldots, J$$
$$W_1 = V_1 \tag{8}$$

Here W_1 corresponds to the coarsest approximation, and it is the vector space of piecewise linear functions associated with vertex nodes in the initial mesh.

To implement the multilevel preconditioner, stiffness matrices $\boldsymbol{A}_k$ are defined for each level W_k and partitioned according to the recursive definition of $\boldsymbol{W}_k$ given in Eq. (8). This is better understood by considering the following definitions of the matrices involved:

$$\boldsymbol{A}_k = \begin{bmatrix} \boldsymbol{A}_{k-1} & \boldsymbol{C}_k^t \\ \boldsymbol{C}_k & \boldsymbol{B}_k \end{bmatrix}$$
$$A_k^{ij} = a(\phi_i, \phi_j), \qquad \phi_i, \phi_j \in W_k$$
$$B_k^{ij} = a(\phi_i, \phi_j), \qquad \phi_i, \phi_j \in V_k$$
$$C_k^{ij} = a(\phi_i, \phi_j), \qquad \phi_i \in V_k, \phi_j \in W_{k-1} \tag{9}$$

The PCG algorithm requires only the action of the preconditioner on a given vector $\boldsymbol{g}$, and therefore it is not necessary to explicitly construct or store the preconditioner. Using the preceding definitions, the multilevel preconditioner, $\boldsymbol{N}_J$, is constructed recursively. To compute $\boldsymbol{N}_J\boldsymbol{g}$, the following inexact factorization $\boldsymbol{M}_k$ of $\boldsymbol{A}_k$ for $k = 2, \ldots, J$ is defined:

$$\boldsymbol{M}_k = \begin{bmatrix} \boldsymbol{M}_{k-1} & \boldsymbol{C}_k^t \\ 0 & \boldsymbol{B}_k \end{bmatrix} \begin{bmatrix} \boldsymbol{I} & 0 \\ \boldsymbol{B}_k^{-1}\boldsymbol{C}_k & \boldsymbol{I} \end{bmatrix} \tag{10}$$

Comparison of Eq. (9) with Eq. (10) shows that $\boldsymbol{M}_{k-1}$ is intended to be an approximation to $\boldsymbol{S}_k$. Because of the form of $\boldsymbol{M}_k$, an inverse $\boldsymbol{M}_k^{-1}$ may be written in terms of the submatrices $\boldsymbol{M}_{k-1}, \boldsymbol{B}_k, \boldsymbol{C}_k$. This inverse defines the preconditioner $\boldsymbol{N}_k$ for $\boldsymbol{A}_k$ corresponding to a particular hierarchical level k. Here, we take $\boldsymbol{N}_k\boldsymbol{g} = \boldsymbol{M}_k^{-1}\boldsymbol{g}$ and note that to compute $\boldsymbol{M}_k^{-1}$, it is necessary to compute $\boldsymbol{M}_{k-1}^{-1}$ corresponding to the next coarser mesh level. This illustrates the recursive nature of the preconditioner. Note that for the recursion to make sense, $\boldsymbol{M}_1$ must be defined. Many variants of the defined preconditioner may be efficiently implemented. Primarily, these variants attempt to reduce the expense of the preconditioner by reducing memory and cpu time while still maintaining the integrity of the preconditioner.

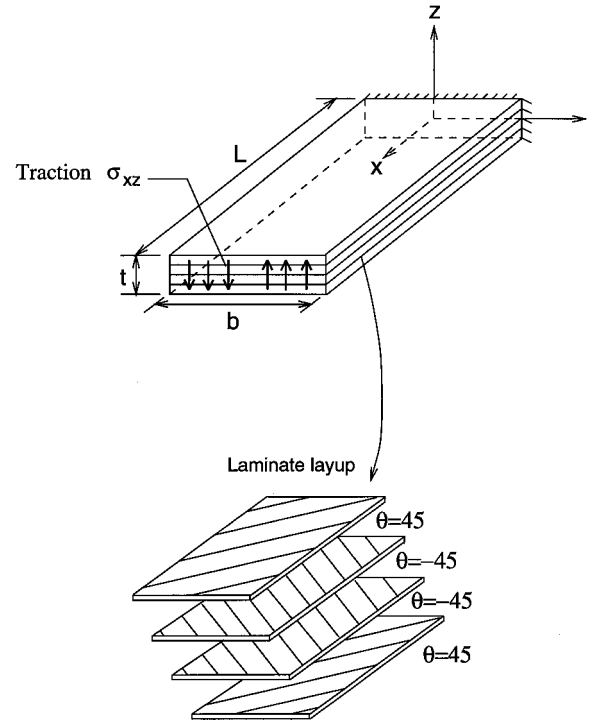

Fig. 3 Torsion of a cantilevered laminate; geometry, lamination scheme, and loading.

III. Analysis of the Torsion Problem

A. Analysis Using the Three-Dimensional Model

Laminates subjected to torsional loading conditions are numerically analyzed here. A cantilevered $(45/-45)_s$ laminate, as shown in Fig. 3, is subjected to a traction $t_z = \sigma_{xz}$ that tends to produce a twisting moment about the x axis. The traction σ_{xz} is assumed to be of the form

$$\sigma_{xz} = 3C_t(t/b)(y/b)[1 - (2z/t)^2] \tag{11}$$

where t is the total thickness of the laminate, b is the width, and C_t is a scaling parameter. The torque about the x axis is given by

$$T = \int_{-t/2}^{t/2}\int_{-b/2}^{b/2} \sigma_{xz} y \, \mathrm{d}y \, \mathrm{d}z = \frac{bt^2}{6} C_t \tag{12}$$

A value of $C_t = 100$ psi is used in the study. The material properties of individual layers in the principal material coordinates are taken to be

$$E_1 = 2.5 \times 10^7 \text{ psi}, \quad G_{12} = 5 \times 10^5 \text{ psi}, \quad \nu_{12} = 0.25$$
$$E_2 = 1.0 \times 10^6 \text{ psi}, \quad G_{23} = 2 \times 10^5 \text{ psi}, \quad \nu_{23} = 0.25$$
$$E_3 = 1.0 \times 10^6 \text{ psi}, \quad G_{31} = 5 \times 10^5 \text{ psi}, \quad \nu_{31} = 0.01 \tag{13}$$

Very refined, uniform meshes were used to compute stresses for five different span ratios $b/t = 1$, 2, 4, 8, and 16 (Figs. 4–6). The particulars of the mesh for all cases are given in Table 1, where (N_x, N_y, N_z) denote the number of elements in the three coordinate directions. Convergence studies were performed by increasing the polynomial order of approximation on each element from $p = 2$ to 4 and in one case up to $p = 5$. The CG algorithm was used for solving the block diagonal problems (inner iteration), and the tolerance for solving these problems was investigated. The rate of convergence of the outer iteration, corresponding to the PCG solve, is affected by

Table 1 Torsion of a cantilevered laminate; mesh details (see Figs. 3–6)

Problem no.	b, in.	L, in.	N_x	N_y	N_z
1 ($b/t=1$)	1	8	32	8	8
2 ($b/t=2$)	2	4	32	16	8
3 ($b/t=4$)	4	4	32	16	8
4 ($b/t=8$)	8	8	24	24	8
5 ($b/t=16$)	16	16	32	32	8

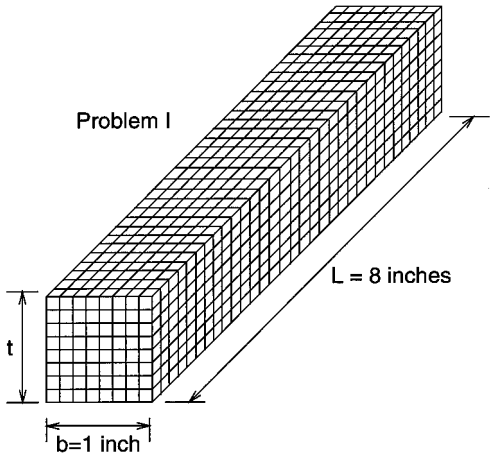

Problem I: $b/t = 1$

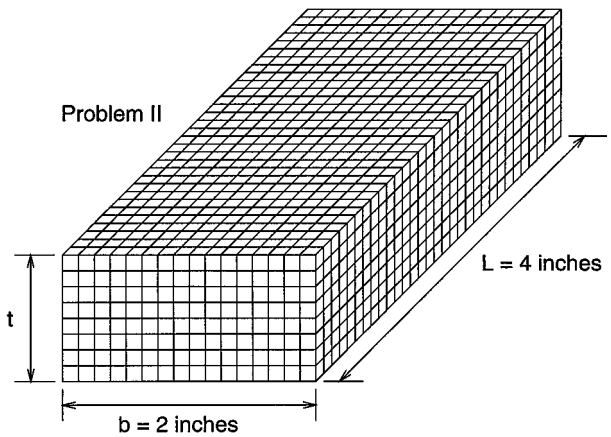

Problem II: $b/t = 2$

Fig. 4 Three-dimensional meshes used for the torsion problem.

the quality of the solution produced by the inner iteration. Effective solution of the inner problems depends on the conditioning of the block diagonals. The results of these studies can be found in Ref. 26. The discussion here is limited to the stress fields obtained.

The interlaminar stresses σ_{zz} and σ_{xz} are of primary concern to design engineers because they are one of the contributing factors to delaminations in laminates subjected to torsional loads. The main characteristics of the stress distributions were found to be the same in all cases. For all span ratios $b/t = 1, 2, 4, 8,$ and 16, the maximum value for σ_{xz} was found to occur at the free edge (refer to Figs. 3 and 7) corresponding to the geometric midplane of the laminate ($y = -b/2$, $z = 0$). The maximum value for σ_{zz} also occurs at the free edge, although it is located at the $(45/-45)$ interfaces. As a rule, stresses computed at the so-called reduced Gauss points on the element are known to be the most accurate. As such, stresses were computed along lines A–A, B–B, and C–C, as shown in the schematic of a typical laminate cross section given in Fig. 7.

Figures 8 and 9 show the distribution of σ_{zz} and σ_{xz}, respectively, across the width for three different positions along the length ($x = L/4$, $L/2$, $3L/4$) of the laminate with $b/t = 1$, and they are the same at each location. This result is reasonable, considering that the laminate length L is eight times larger than the width, while the cross section is square.

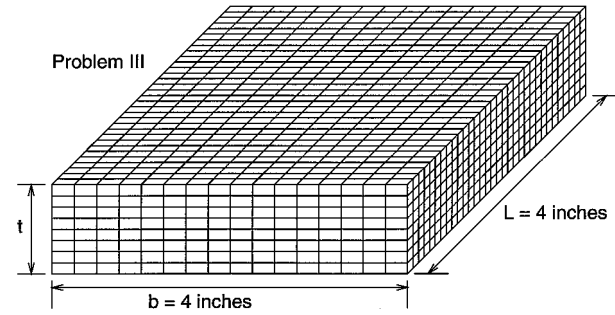

Problem III: $b/t = 4$

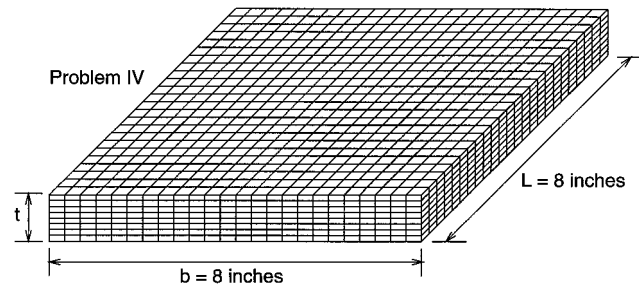

Problem IV: $b/t = 8$

Fig. 5 Three-dimensional meshes used for the torsion problem.

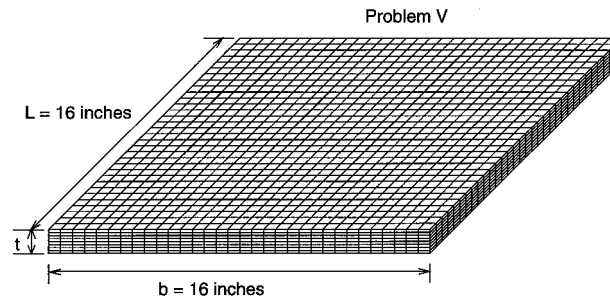

Fig. 6 Three-dimensional mesh used for the torsion problem V: $b/t = 16$.

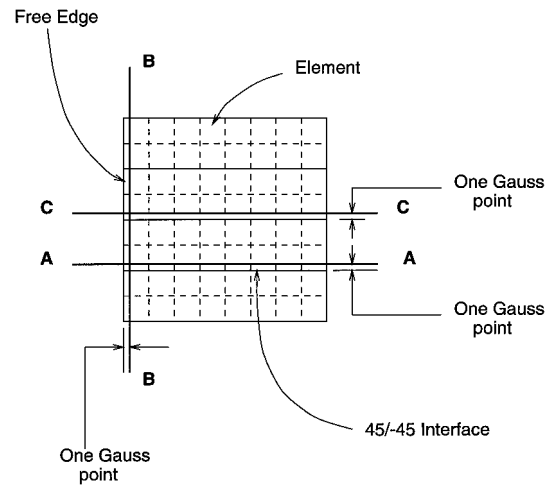

Fig. 7 Locations for stress computations in $(45/-45)_s$ laminate.

The nature of the stress distributions for the remaining cases was identical to those shown for case $b/t = 1$, and therefore only the through-thickness variation at B–B of the interlaminar stresses for cases $b/t = 2, 4, 8,$ and 16 and $x = L/2$ are shown in Figs. 10 and 11. For these cases, the laminate is either a plate or a beam rather than a three-dimensional solid, hence it is expected that the stresses are not uniform along the length, as shown in Figs. 12 and 13 for $b/t = 16$ at $x = L/4$, $L/2$, and $3L/4$.

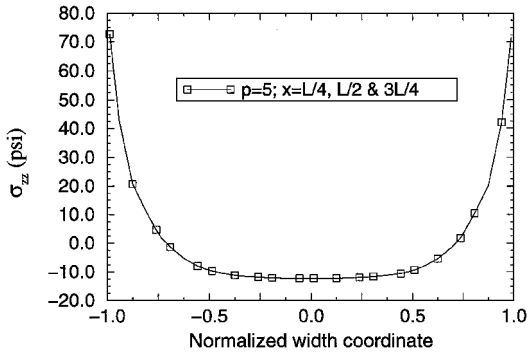

Fig. 8 Distribution of stress σ_{zz} along A–A of the $(45/-45)_s$ laminate ($b/t = 1$).

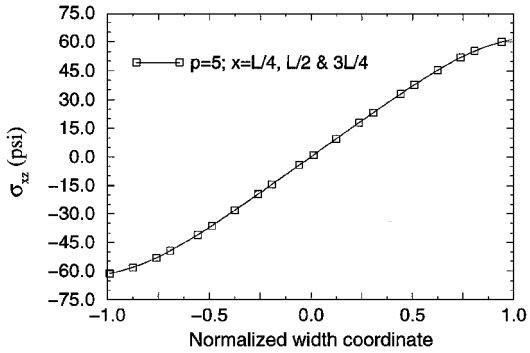

Fig. 9 Distribution of stress σ_{xz} along C–C of the $(45/-45)_s$ laminate ($b/t = 1$).

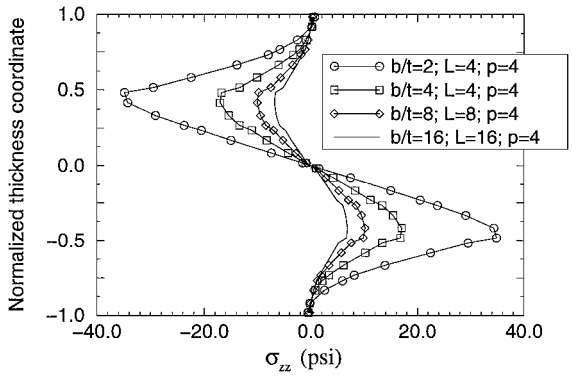

Fig. 10 Distribution of stress σ_{zz} along B–B at $x = L/2$ of the $(45/-45)_s$ laminate for $b/t = 2$, 4, 8, and 16.

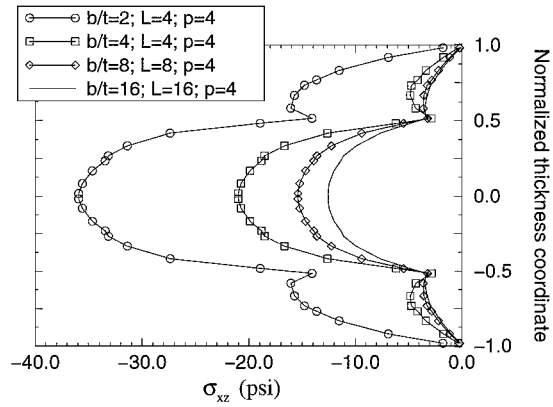

Fig. 11 Distribution of stress σ_{xz} along B–B at $x = L/2$ of the $(45/-45)_s$ laminate for $b/t = 2$, 4, 8, and 16.

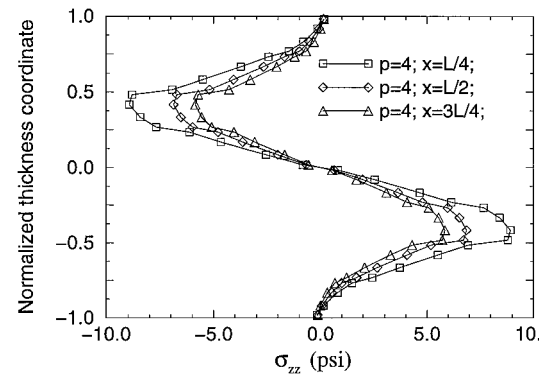

Fig. 12 Distribution of stress σ_{zz} along B–B at $x = L/4$, $L/2$, $3L/4$ of the $(45/-45)_s$ laminate for $b/t = 16$.

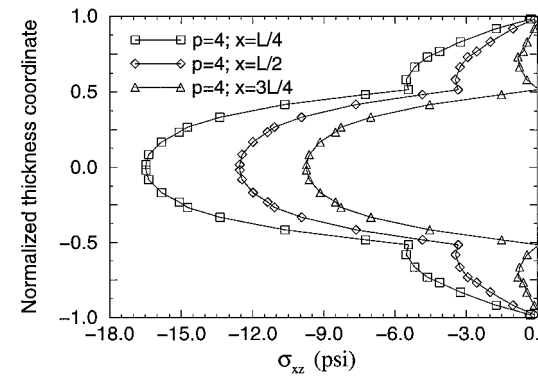

Fig. 13 Distribution of stress σ_{xz} along B–B at $x = L/4$, $L/2$, $3L/4$ of the $(45/-45)_s$ laminate for $b/t = 16$.

B. Analysis Using a Quasi-Three-Dimensional Model

To reduce the computational cost of a fully three-dimensional analysis, quasi-three-dimensional models have been developed. The quasi-three-dimensional model assumes a laminate loaded by tractions applied only on its ends, along the x direction, such that stress components are independent of x (see Fig. 14). Based on these assumptions, integration of the equilibrium equations will yield a simplified displacement field.[15] This displacement field may be used to construct a two-dimensional finite element model, in which strains are functions of (y, z) only, so that it is only necessary to model the y–z plane.

The following displacement field is assumed:

$$u(x, y, z) = -(C/2)yz + \left(Ky + K_x z + \varepsilon_x^0\right)x + U(y, z)$$

$$v(x, y, z) = (K_{xy}/2)xz - (K/2)x^2 + V(y, z)$$

$$w(x, y, z) = -(K_{xy}/2)xy + S_b x - (K_x/2)x^2 + W(y, z) \tag{14}$$

where K denotes out-of-plane bending curvature about the z axis; ϵ_x^0, the extensional strain along the x axis; K_x, the in-plane bending curvature about the y axis; K_{xy}, the twisting curvature about the x axis; and S_b, the transverse shear strain due to transverse shear loading. In the Chan and Ochoa model,[16] $C = 0$, whereas in the Leger and Chan model[17] $C = K_{xy}$. The displacement field of Eq. (14) can be used in the Navier equations of elasticity and an associated displacement finite element model with (U, V, W) as the nodal variables can be developed.[27]

The parameters ϵ_x^0, K, K_x, K_{xy}, S_b serve as the data in the model, and physically meaningful values of these parameters may be computed for a specific problem using the classical laminate theory ideas treated in the books by Jones[28] and Reddy.[25] Symmetric angle-ply laminates exhibit coupling between the bending and twisting curvatures so that for a pure torsional loading condition, there will be nonzero values for both K_x and K_{xy}. This can be verified upon inspection of the ABD matrices. Of course, there is also a nonzero value for K_y, but that does not contribute to this model. The uniform

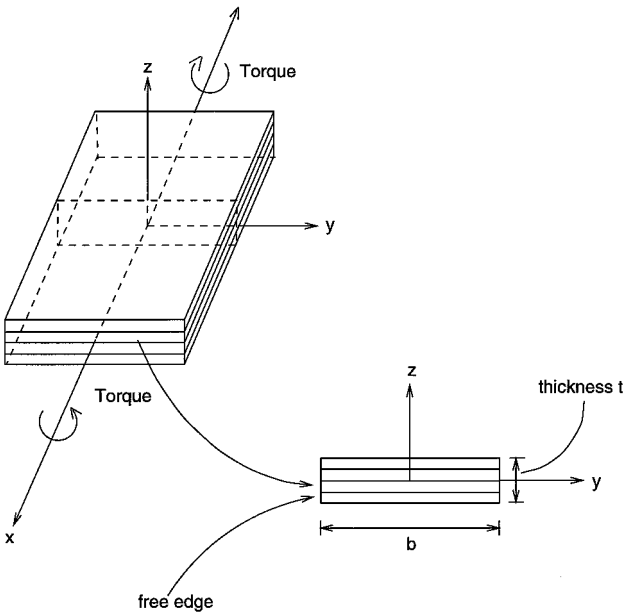

Fig. 14 Torsion of a cantilevered laminate (quasi-three-dimensional model).

axial strain ϵ_x^0 does not couple with the bending and twisting curvatures for symmetric laminates and was taken as zero here. The constants K and S_b are not part of the classical laminate theory and by default do not couple with ϵ_x^0, K_x, K_{xy}. However, using some assumptions, values for K and S_b may be computed,[17] although in the present analysis they were taken as zero. Orthotropic material properties of an individual lamina are assumed to be the same as those given in Eq. (13).

Boundary conditions for the torsion problem are taken as

$$U(0,0) = V(0,0) = W(0,0) = 0 \tag{15}$$

These boundary conditions do not eliminate all rigid body modes, and the system is nearly singular. Direct solution of the equations leads to significant round-off error. Because of these facts, it is necessary for practical purposes to use an iterative solution procedure. The CG algorithm suits this purpose.

Pure torsional loading conditions are considered here. To use the classical laminate theory for computing the constants K_x and K_{xy}, it is necessary to have a torsional resultant M_{xy} (measured per unit width). To make comparisons with results obtained using the three-dimensional model discussed above, the value used for M_{xy} is chosen as

$$M_{xy} = C_t t^2 \big/ 6 \tag{16}$$

The total torque T on the laminate is found by integrating M_{xy} along the width. Because M_{xy} is constant, T is the same as that given in Eq. (12). The torsional resultant M_{xy}, along with the resulting curvatures obtained from the classical laminate theory, are

$$C_t = 100, \qquad M_{xy} = 16.67 \text{ lb-in./in.}$$
$$K_x = 2 \times 10^{-5}, \qquad K_{xy} = -5.957 \times 10^{-5} \tag{17}$$

The $(45/-45)_s$ laminate that was studied previously using the three-dimensional model is analyzed using the quasi-three-dimensional model. Interlaminar stresses σ_{zz} and σ_{xz} from the quasi-three-dimensional models are compared with those obtained using the three-dimensional model for the case of $b/t = 16$. Each lamina has equal thickness, and there are two elements per lamina in the thickness direction. For comparison purposes, the mesh (refer to Fig. 15) used for the quasi-three-dimensional model corresponds to the mesh used in the $y-z$ plane of the three-dimensional model (refer to Fig. 6).

Results of stress calculations along B–B (refer to Fig. 7) are shown in Figs. 16 and 17. The elasticity solution refers to the results of the three-dimensional model presented earlier for a laminate of

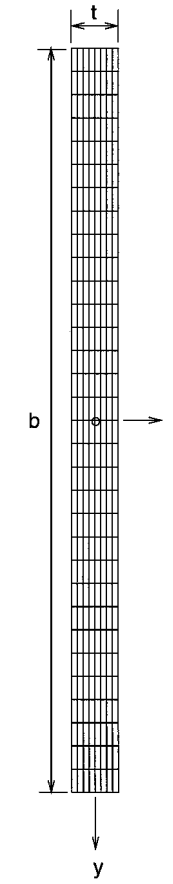

Fig. 15 Mesh used for the quasi-three-dimensional model of the $(45/-45)_s$ laminate; $b/t = 16$; $t = 1$ in.; B.C.: $U = V = W = 0$ at $y = z = 0$.

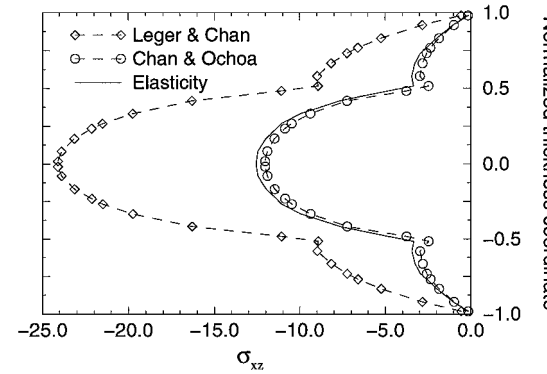

Fig. 16 Comparison of stress σ_{zz} from various models (all results obtained in the present study), results of the three-dimensional model were obtained at $x = L/2$ with $L = 16$ in. ($b/t = 16$ and $t = 1$ in.).

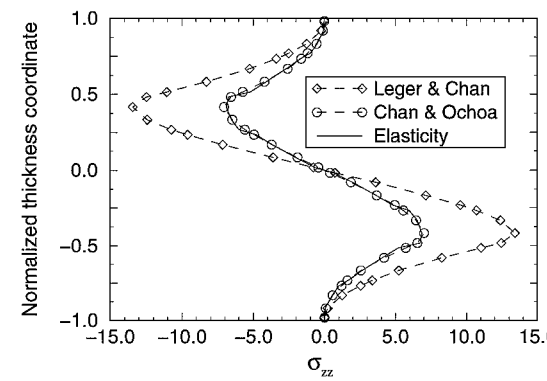

Fig. 17 Comparison of stress σ_{xz} from various models. Results of the three-dimensional model were obtained at $x = L/2$ with $L = 16$ in. ($b/t = 16$ and $t = 1$ in.).

length $L = 16$ at $x = L/2$. This location is the most reasonable place to make comparisons between the three-dimensional elasticity and quasi-three-dimensional models, because it is the location farthest away from the cantilevered end and the end on which tractions are applied. Note the close agreement between the present quasi-three-dimensional results based on the Chan and Ochoa model[16] and those obtained using the three-dimensional elasticity model. For laminates in which there is no twisting/bending coupling, the Leger and Chan model[17] is exactly 50% in error for torsional load cases, because, in these cases, only twisting curvature contributes to the the interlaminar shear strain ϵ_{xz}. In such cases, the induced strain ϵ_{xz} is twice as large as it apparently should be, as shown by results using the three-dimensional elasticity model. One way of thinking about this error is to consider the extra term $-(C/2)yz$ in the displacement field for the quasi-three-dimensional model, as already accounted for by $U(y, z)$. Because of this discrepancy, the Leger and Chan model will not be considered further.

The symmetric, four-ply laminates discussed earlier are further studied with refined meshes and higher values of p. Two laminates, corresponding to the geometric ratios $b/t = 8$ and $b/t = 16$ are considered here, as indicated by the finite element meshes in Fig. 18. There are two elements per lamina in the thickness direction. To keep element span ratios equal to one, the number of elements in the y direction was taken as 64 and 128 for the span ratios $b/t = 8$ and $b/t = 16$, respectively.

The polynomial order of interpolation p was increased from $p = 2$ to 8 and $p = 2$ to 6 for the cases $b/t = 8$ and $b/t = 16$, respectively.

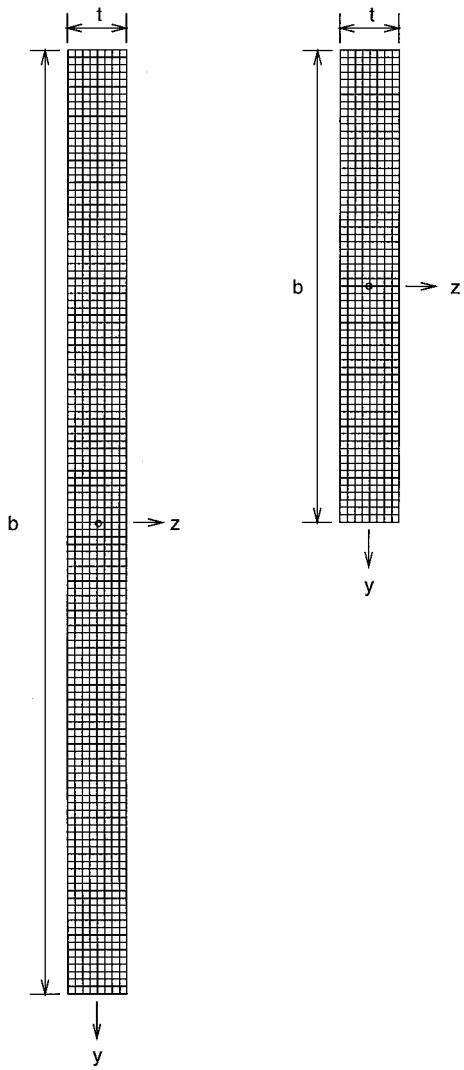

Fig. 18 Meshes used for the quasi-three-dimensional model of the $(45/-45)_s$ laminate; $b/t = 8$ and $b/t = 16$, $t = 1$ in.; B.C.: $U = V = W = 0$ at $y = z = 0$.

The preconditioner was constructed using the hierarchical vector spaces defined for quadrilateral elements, as described earlier. The CG solver was used for inner iterations on level 1, and direct solvers were used for the remaining hierarchical levels. The absolute stopping criterion was used for the inner iteration on the bottom level with a tolerance of $\epsilon = 1 \times 10^{-10}$. The outer iteration, corresponding to the PCG solve, used the absolute stopping criterion with a stopping tolerance of $\epsilon = 1 \times 10^{-11}$.

Overall, the iterative solution procedures performed very well for the problems studied. The number of iterations required for convergence is generally low. Although the domain is two-dimensional, large problems still arise because of the extent to which p is increased and also because the model has three nodal variables (U, V, W). The total number of degrees of freedom for the meshes used here range in size from 6579 to 113,043.

Stresses were computed for all values of p in both laminates (i.e., $b/t = 8$ and $b/t = 16$). Locations for stress calculations were chosen where the stresses were thought to be maximum (free edge). As with previous stress calculations, the stresses were evaluated at the reduced Gauss points, namely along lines A–A, B–B, and C–C, as indicated in Fig. 7. The line B–B is always in the first column of elements on the left of the mesh, and is situated one Gauss point to the right of the free edge. The line A–A is situated in the second lamina from the bottom at a distance above the $45/-45$ interface corresponding to one Gauss point. This is the third row of elements from the bottom. Finally, the line C–C is located along the midplane of the laminate as shown. The intersection of B–B and C–C is where the interlaminar shear stress σ_{xz} reaches a maximum. In general, the geometric locations of these lines depend on the number of Gauss points used to calculate the stresses. If the polynomial order on the element is p, then the pth Gauss rule was used for stress computations. The lines move slightly depending upon p. In all cases, there is always one point in common between the plots along A–A and B–B (similarly for C–C and B–B), and this was used as a check.

Interlaminar stress distributions for both laminates, $b/t = 8$ and $b/t = 16$, are given in Figs. 19 and 20. It is useful to compare the

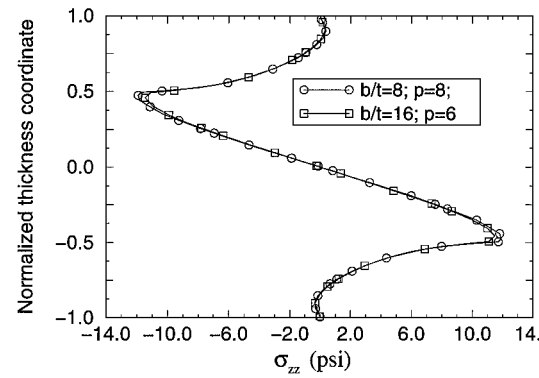

Fig. 19 Distribution of stress σ_{zz} through the thickness (along B–B) of the $(45/-45)_s$ laminate ($b/t = 8$ and $b/t = 16$; $t = 1$ in.).

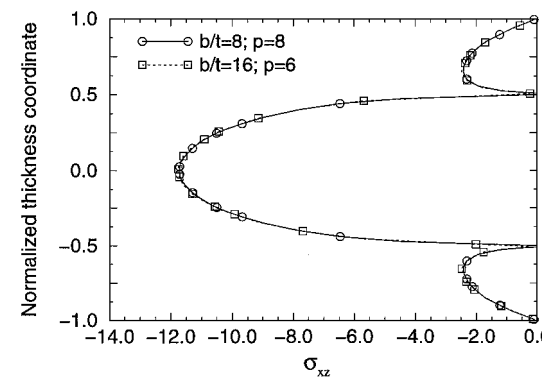

Fig. 20 Distribution of stress σ_{xz} through the thickness (along B–B) of the $(45/-45)_s$ laminate ($b/t = 8$ and $b/t = 16$; $t = 1$ in.).

stresses obtained here with those obtained in preceding sections using the three-dimensional elasticity model with lower values of p. Results obtained using the quasi-three-dimensional model are qualitatively identical to those obtained using the three-dimensional elasticity model. There are differences in some of the maximum values for stresses. For example, compare Fig. 12 with Fig. 19. The maximum value obtained for σ_{zz} with the elasticity model ($b/t = 16$, $p = 4$) is approximately 7 psi, whereas the quasi-three-dimensional model predicts 12 psi. This difference can be attributed to the fact that the locations at which stresses are computed in each case is different as a result of element geometry and the Gauss rule. As p increases, the first Gauss point tends to move toward the free edge. Because σ_{zz} is changing so rapidly at the free edge, small changes in the location at which the stress is calculated can result in moderate to large changes in the computed value for the stress.

As shown in Figs. 13 and 20, the maximum value for σ_{xz} using both the three-dimensional elasticity and quasi-three-dimensional models was found to be the same. However, note the sharp cusplike form that the quasi-three-dimensional model predicts for σ_{xz}. This structure is present in the three-dimensional elasticity results, but it is not nearly as sharp. This lack of sharpness may be due to the fact that the polynomial order is at $p = 4$ (three-dimensional elasticity model) rather than at the higher level of $p = 6$ or 8 in the quasi-three-dimensional results.

IV. Conclusions

In this study, a multilevel, recursively defined preconditioner developed by the authors was used to analyze the three-dimensional elasticity and quasi-three-dimensional models of laminated structures subjected to torsional loads. The results obtained with the quasi-three-dimensional model compared well with those obtained with the three-dimensional elasticity model.

The PCG algorithm is an efficient means for solving the algebraic equations arising from finite element discretizations of problems of laminated composite structures. The efficiency of the algorithm strongly depends on the quality of the preconditioner used in the algorithm. The preconditioner was successfully tested in two-dimensional problems up to $p = 8$, and in three dimensions up to $p = 5$, using the serendipity brick elements. In both cases, the number of iterations required for convergence was well within practical limits.

Acknowledgments

The research reported here was supported by the Air Force Office of Scientific Research through Grant F49620-95-1-0342 and the Army Research Office through Grant DAAH 04-96-1-0080. The second author was also supported by the Oscar S. Wyatt Endowed Chair during the course of this study.

References

[1]Bramble, J. H., Pasciak, J. E., and Schatz, A. H., "The Construction of Preconditioners for Elliptic Problems by Substructuring, IV," *Journal of Mathematics of Computation*, Vol. 53, 1989, pp. 1–24.

[2]Bramble, J. H., Pasciak, J. E., and Xu, J., "Parallel Multilevel Preconditioners," *Third International Symposium on Domain Decomposition Methods for Partial Differential Equations*, edited by R. Glowinski, J. Periaux, and O. B. Widlund, Society for Industrial and Applied Mathematics, Philadelphia, 1989, pp. 341–357.

[3]Bramble, J. H., *Multigrid Methods*, Longman (copublished in the United States with Wiley, New York), 1993.

[4]Briggs, W. L., *A Multigrid Tutorial*, Society for Industrial and Applied Mathematics, Philadelphia, 1987.

[5]Hackbusch, W., and Trottenberg, U., *Multigrid Methods*, Springer-Verlag, Berlin, 1992.

[6]Wesseling, P., *An Introduction to Multigrid Methods*, Wiley, New York, 1992.

[7]Bank, R. E., "Hierarchical Bases and the Finite Element Method," *Acta Numerica 1996*, edited by A. Iserles, Cambridge Univ. Press, Cambridge, England, U.K., 1996, pp. 1–43.

[8]Bank, R. E., Dupont, T., and Yserentant, H., "The Hierarchical Basis Multigrid Method," *Numerische Mathematik*, Vol. 52, No. 4, 1988, pp. 427–458.

[9]Yserentant, H., "Two Preconditioners Based on the Multilevel Splitting of Finite Element Spaces," *Numerische Mathematik*, Vol. 58, No. 2, 1990, pp. 163–184.

[10]Axelsson, O., and Vassilevski, P. S., "Algebraic Multilevel Preconditioning Methods, II," *SIAM Journal on Numerical Analysis*, Vol. 27, No. 6, 1990, pp. 1569–1590.

[11]Mandel, J., "Two-Level Domain Decomposition Preconditioning for the $p-$Version Finite Element Method in Three Dimensions," *International Journal for Numerical Methods in Engineering*, Vol. 29, No. 5, 1990, pp. 1095–1108.

[12]Axelsson, O., *Iterative Solution Methods*, Cambridge Univ. Press, New York, 1994, pp. 252–302 and 449–501.

[13]Saint-Georges, P., Warzee, G., Beauwens, R., and Notay, Y., "High-Performance PCG Solvers for FEM Structural Analysis," *International Journal for Numerical Methods in Engineering*, Vol. 39, No. 8, 1996, pp. 1313–1340.

[14]Reddy, J. N. (ed.), *Mechanics of Composite Materials*, Kluwer, Dordrecht, The Netherlands, 1994, pp. 287–303.

[15]Pipes, B., and Pagano, N. J., "Interlaminar Stresses in Composite Laminates Under Uniform Axial Extension," *Journal of Composite Materials*, Vol. 4, Oct. 1970, pp. 538–540.

[16]Chan, W. S., and Ochoa, O. O., "Delamination Characterization of Laminates Under Tension, Bending and Torsion Loads," *Computational Mechanics*, Vol. 6, 1990, pp. 393–405.

[17]Leger, C. A., and Chan, W. S., "Analysis of Interlaminar Stresses in Symmetric and Unsymmetric Laminates Under Various Loadings," *Proceedings of the 34th AIAA/ASME/ASCE/AHS/ASC Structures, Structural Dynamics, and Materials Conference*, AIAA, Washington, DC, 1993, pp. 1770–1776.

[18]Liao, W., and Sun, C. T., "Torsional Response of Multilayer Thick Laminates Using Effective Moduli," *Composite Structures*, Vol. 30, No. 1, 1995, pp. 61–68.

[19]Sen, J. K., and Fish, J. C., "Failure Prediction of Composite Laminates Under Torsion," *Key Engineering Materials*, Vol. 120/121, 1996, pp. 285–306.

[20]Fish, J. C., and Marcucelli, K. T., "Interlaminar Fracture of Graphite/Epoxy Laminates Under Torsion Load," *Proceedings of the 34th AIAA/ASME/ASCE/AHS/ASC Structures, Structural Dynamics, and Materials Conference*, AIAA, Washington, DC, 1993, pp. 1343–1351.

[21]Reddy, J. N., and Rasmussen, M. L., *Advanced Engineering Analysis*, Wiley, New York, 1982; reprint, Krieger, Malabar, FL, 1991, pp. 204–214.

[22]Reddy, J. N., *Applied Functional Analysis and Variational Methods in Engineering*, McGraw-Hill, New York, 1986; reprint, Krieger, Malabar, FL, 1991, pp. 135–142.

[23]Reddy, J. N., *An Introduction to the Finite Element Method*, 2nd ed., McGraw–Hill, New York, 1993, pp. 33–35.

[24]Reddy, J. N., *Energy and Variational Methods in Applied Mechanics*, Wiley, New York, 1984, pp. 247–302.

[25]Reddy, J. N., *Mechanics of Laminated Composite Plates: Theory and Analysis*, CRC Press, Boca Raton, FL, 1997, pp. 135–154 and 491–581.

[26]Mitchell, J. A., "A High Performance Iterative Solution Procedure for Solving Problems in Structural Mechanics Using the Finite Element Method," Ph.D. Dissertation, Mechanical Engineering Dept., Texas A&M Univ., College Station, TX, 1997.

[27]Heyliger, P. R., and Reddy, J. N., "Reduction of Free Edge Stress Concentration in Symmetric Composite Laminates," *Journal of Applied Mechanics*, Vol. 52, Dec. 1985, pp. 801–805.

[28]Jones, R. M., *Mechanics of Composite Materials*, Hemisphere, New York, 1975, pp. 147–156.

G. A. Kardomateas
Associate Editor